Chemical Geology 585 (2021) 120563

Contents lists available at ScienceDirect

Chemical Geology

journal homepage: www.elsevier.com/locate/chemgeo

Late diagenetic evolution of Ordovician limestones in the Baltoscandian basin revealed through trace-element mapping and in situ U–Pb dating of calcite

Graham Hagen-Peter [a,*], Yue Wang [a], Olle Hints [b], Anthony R. Prave [c], Aivo Lepland [a,b]

[a] Geological Survey of Norway, Norway
[b] Tallinn University of Technology, Estonia
[c] University of St Andrews, Scotland, UK

ARTICLE INFO

Editor: Claudia Romano

Keywords:
LA-ICP-MS calcite U–Pb dating
LA-ICP-MS trace-element mapping
Tectonic-driven diagenesis
Baltoscandian basin

ABSTRACT

Carbonate rocks are important paleo-environmental records, with bulk chemical and isotopic compositions commonly used to deduce temperatures, redox conditions, etc. Diagenetic (re)crystallization of clasts and cements is common, may perturb the chemical and isotopic systems typically interpreted to reflect conditions at the timing of deposition, may occur essentially synchronous with or long after deposition, and is difficult to date. Advances in in situ carbonate trace-element mapping and U–Pb dating by LA-ICP-MS provide opportunities to determine the absolute timing of diagenesis which can then be related to the age of deposition of carbonate rocks. We applied these techniques to two samples of well-preserved Ordovician bioclastic limestones from the Viki drill core, western Estonia (Baltoscandian basin) with precisely constrained depositional ages (ca. 459 and 444 Ma) and comprehensively detailed post-depositional histories which indicate that they were never deeply buried nor significantly heated following deposition. Previously published K–Ar data for K-bentonites from the Viki core and elsewhere in the Baltoscandian basin do, however, indicate diagenesis long before the timing of maximum burial. Optical petrography and backscatter-electron ("BSE") imaging reveal low-porosity "BSE-bright" calcite spar cement in pore spaces between "BSE-dark" micro-porous carbonate bioclasts. Trace-element mapping of several areas (several mm^2 each) in each thin section by LA-quadrupole-ICP-MS reveals variably elevated Mn/Sr, U concentration, and $^{238}U/^{206}Pb$ in the calcite spar cement. These maps were subsequently used to guide the placement of laser spots for U–Pb dating by LA-multicollector-ICP-MS. Primary bioclastic carbonate in both samples has low U/Pb_c (with $^{238}U/^{206}Pb < \sim 6.5$) and, thus, yields imprecise Concordia-intercept dates, which nonetheless overlap with the depositional ages. Calcite spar cement has higher U/Pb_c (with $^{238}U/^{206}Pb$ up to ~15.7) and yields intercept dates of ca. 414–412 Ma in each sample. Individual common-Pb-corrected dates—particularly those for domains with the highest U/Pb_c—are as young as ca. 376 Ma. The timing of diagenetic calcite (re)crystallization and cementation identified here is tens of Myr later than deposition and overlaps with the previously published K–Ar dates, and also with the timing of continent collision during the Caledonian orogeny in Scandinavia. The calcite U–Pb and K-bentonite K–Ar chronometers yield consistent records of what may have been tectonic-driven diagenesis far inboard (>600 km) from the orogenic front. Furthermore, this work demonstrates that apparently pristine carbonates may have experienced recrystallization (or at least chemical-isotopic perturbation) in open systems long after deposition and should be carefully scrutinized before using bulk-sample paleoenvironmental proxies.

1. Introduction

Primary (i.e., depositional) carbonate phases in limestones archive a wealth of geochemical information about environmental conditions at the time of formation. These, however, can become compromised by diagenesis that may occur soon after deposition (e.g., Bathurst, 1976) or

* Corresponding author.
E-mail addresses: graham.hagen-peter@ngu.no (G. Hagen-Peter), yue.wang@ngu.no (Y. Wang), olle.hints@taltech.ee (O. Hints), ap13@st-andrews.ac.uk (A.R. Prave), aivo.lepland@ngu.no (A. Lepland).

https://doi.org/10.1016/j.chemgeo.2021.120563
Received 22 July 2021; Received in revised form 29 September 2021; Accepted 3 October 2021
Available online 5 October 2021

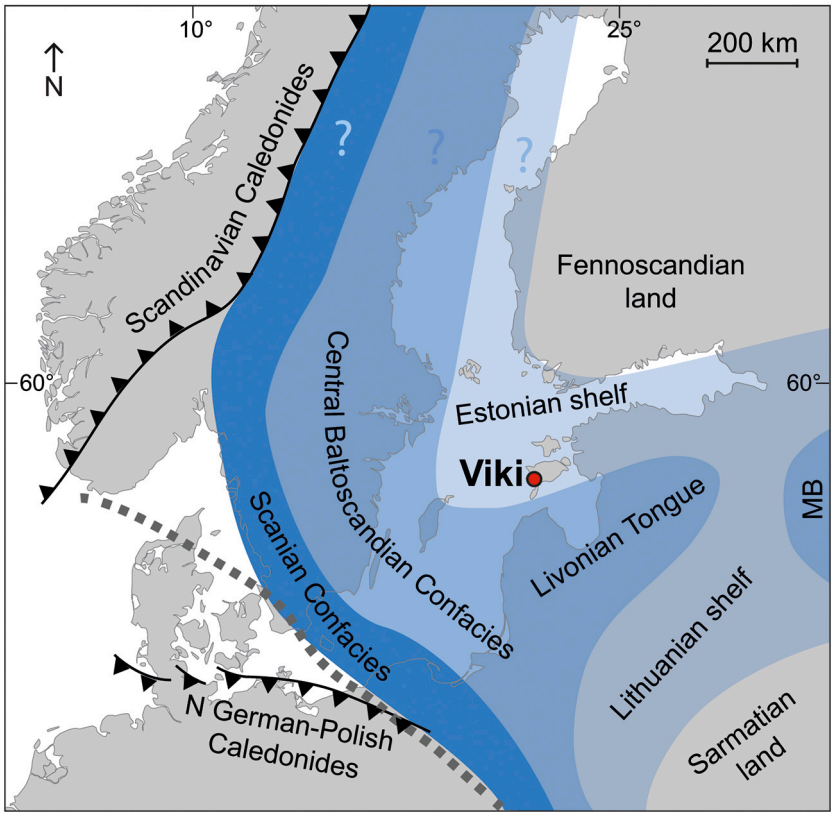

Fig. 1. Map showing the extent and simplified configuration of the Baltoscandian basin during the Ordovician and the location of the Viki drill site within the main facies belts. Compiled after Jaanusson (1995), Männil (1966) and Środoń et al. (2009). Abbreviations are as follows: "MB": Moscow Basin.

millions of years later (e.g., Smith et al., 1991; Godeau et al., 2018), be protracted or punctuated, and also be complex in terms of conditions and the compositions of diagenetic fluids (Brand and Veizer, 1980; Derry, 2010). Such processes have critical bearing on a multitude of characteristics of the rock ranging from the preservation or perturbation of trace-element and isotopic proxies (Swart, 2015) to the development of porosity and quality of hydrocarbon reservoirs (Godeau et al., 2018). Furthermore, even though absolute timing of deposition can be established via biostratigraphy, isotopic correlation, or radiometric dating of interbedded volcanic strata, determining the absolute timing of diagenetic carbonate (re)crystallization is challenging.

Combined trace-element mapping and in situ U–Pb geochronology of carbonates in thin sections by LA-ICP-MS provides opportunities to assign absolute ages to multiple generations of carbonate (re)crystallization in a sample with petrographic and geochemical context (Roberts and Walker, 2016; Roberts et al., 2020; Drost et al., 2018), with the potential of directly dating diagenetic (re)crystallization (e.g., Godeau et al., 2018). We have applied this approach to two samples of well-preserved Ordovician (ca. 459 and 444 Ma) limestones from the Viki drill core, western Estonia, which provide a case study to evaluate depositional versus diagenetic age in exceptionally well-preserved carbonate rocks. This sequence likely did not experience temperatures above 50 °C since deposition (Kirsimäe et al., 2020) but experienced diagenesis at ca. 420–370 Ma as evident by K–Ar dates for illite-smectite and low-temperature K-feldspar from K-bentonite layers throughout the Baltoscandian basin (Somelar et al., 2009; Środoń et al., 2009). Accordingly, these rocks are exemplary for differentiating the age of well-preserved original textures from those linked to later diagenetic overprinting. Such knowledge is fundamental for guiding interpretation of geochemical data that have become a mainstay in evaluating Earth surface redox conditions, deducing driving mechanisms of environmental and climatic change, and in documenting porosity-permeability in carbonate rocks.

2. Geological background

2.1. The Baltoscandian basin and Viki borehole

The early Paleozoic Baltoscandian basin was an epicontinental seaway in which carbonate deposition was more-or-less continuous from early Ordovician until late Silurian, after which terrigenous sediment sourced from the Scandinavian Caledonides filled the basin as a consequence of collision with eastern Avalonia and Laurentia (Cocks and Torsvik, 2005, 2020). Paleogeographically the basin is subdivided into several facies zones (Fig. 1; "confacies" belts of Männil, 1966; Jaanusson, 1976; Nestor and Einasto, 1997), and its sedimentological evolution records a transition from a cool- and temperate-climate sediment-starved carbonate ramp to a well-differentiated tropical platform-basin system (Nestor and Einasto, 1997).

The Viki drill core comes from western Saaremaa Island, Estonia (58.35107°N, 22.07985°E; Fig. 1). The recovered Ordovician succession (depth range 242.8 to 363.0 m; Fig. 2) is represented by the Dapingian-Hirnantian shallow-water carbonate ramp to carbonate platform stages represented by wackestones, packstones, and marlstones with variable admixtures of terrigenous clay. Near the base of the Katian, sedimentation rate increased and lithofacies became more diverse and include reefs and oolitic grainstones containing a normal marine benthos dominated by echinoderms, bryozoans, brachiopods, trilobites and calcareous algae (Põldvere, 2010). The Viki core has been studied intensively for micropaleontology and biostratigraphy (e.g., Jeppsson and Männik, 1993; Nestor, 2005; Tonarová et al., 2014; Hints et al., 2014), K-bentonites (e.g., Kiipli et al., 2010), and stable isotopes (Kaljo et al., 2003; Hints et al., 2014; Richardson et al., 2019). The main carbon isotope excursions known for the region have been identified in the core

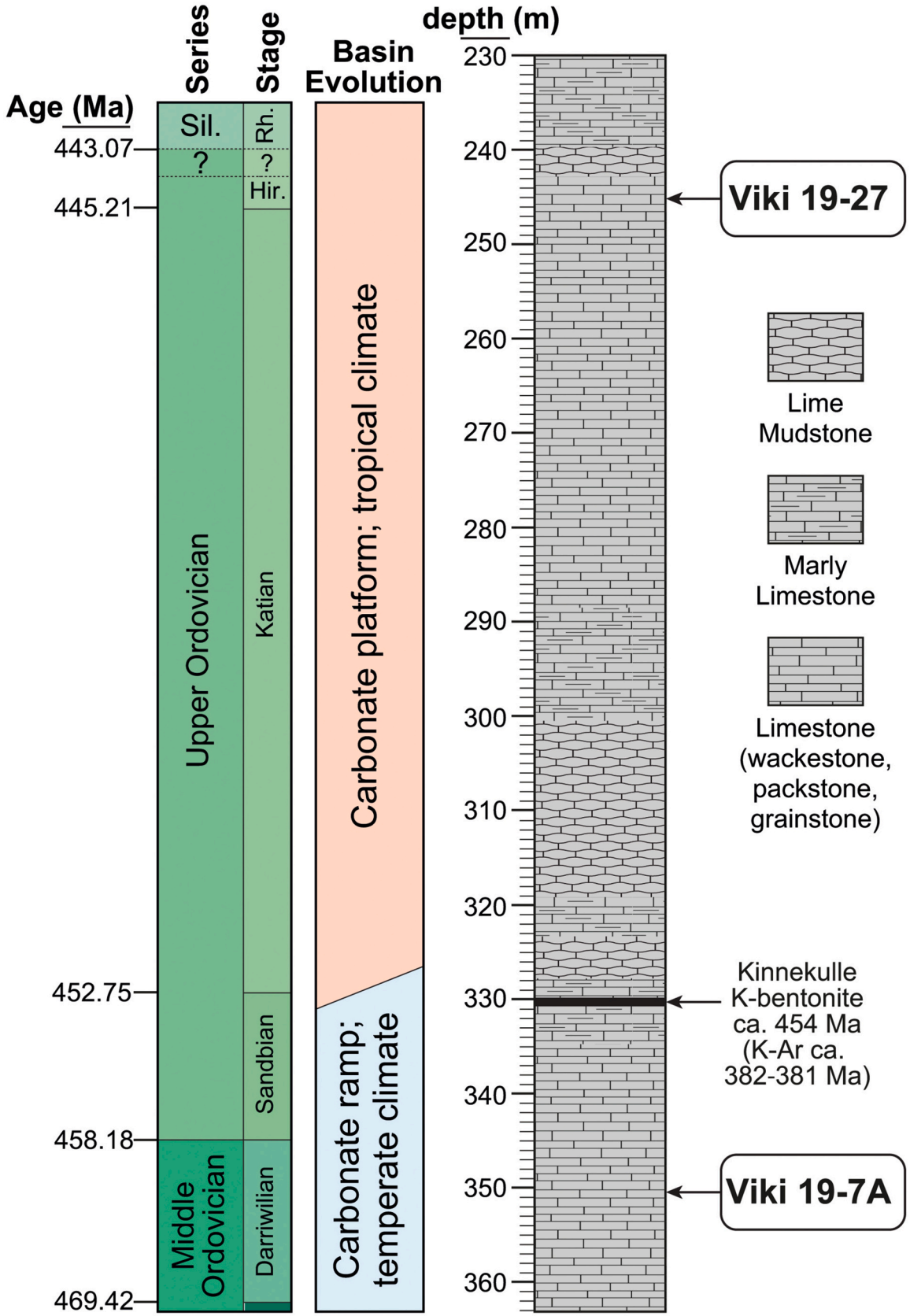

Fig. 2. Generalized stratigraphy of the Ordovician succession of the Viki core showing the positions of samples Viki19-7A and Viki19–27. Further details on the stratigraphy of the section are provided by Hints et al. (2014) and Põldvere (2010). Numerical dates are according to Goldman et al. (2020). Also shown are the inferred eruption age (ca. 454 Ma) and K–Ar dates (interpreted as diagenetic ages; Środoń et al., 2009) of the Kinnekulle K-bentonite. Abbreviations are as follows: "Sil.": Silurian; "Hir.": Hirnantian; "Rh.": Rhuddanian.

(Ainsaar et al., 2010; Hints et al., 2014). Sulfur isotope data on carbonate-associated sulfate ($\delta^{34}S_{CAS}$) and pyrite ($\delta^{34}S_{pyr}$) for early Silurian strata in the core reveal how diagenetic overprints can mask basinal and global signals (Richardson et al., 2019), complementing work done on correlative strata elsewhere in the Baltoscandian basin (e.g., Rose et al., 2019). Such overprints may apply also to the Ordovician part of the carbonate succession in the Viki core.

2.2. Depositional age constraints

The two samples used in this study, Viki19-7A and − 27, come from depths of 350.2 and 245.1 m (Fig. 2). They represent Uhaku and Porkuni regional stages, late Darriwilian and Hirnantian, respectively. Bentonites in the Viki core have not been dated radiometrically, but— based on stratigraphic position, thickness, and geochemical properties—two distinct bentonites can be confidently correlated to the 454.06 ± 0.49 Ma Kinnekulle K-bentonite (Ballo et al., 2019), occurring at 330.3 m depth, and the 438.7 ± 1.0 Ma Osmundsberg K-bentonite (Bergström et al., 2008) at 185.2 m depth. These depositional age constraints can be refined further to ca. 459 and 444 Ma for Viki19-7A and − 27, respectively, using high-resolution biostratigraphy of the Viki section (Põldvere, 2010; Hints et al., 2014) and Baltic Ordovician sequences in general (Nõlvak et al., 2006), as correlated with the time-calibrated international chronostratigraphic scale (e.g., Goldman et al., 2020).

2.3. Post-depositional history

Although no burial history studies have been conducted on the Ordovician carbonate rocks in the Viki core, conodont alteration index (CAI) analyses of Ordovician-Silurian strata in the part of the Baltoscandian basin where the core was obtained are typified by a CAI = 1 (Lehnert et al., 2010); higher values are only found in southern Sweden, Kaliningrad region, and eastern Poland where burial depths reached 4–5 km (Nehring-Lefeld et al., 1997). Furthermore, palynomorph (acritarch) darkness index (PDI) studies applied to assess maturity of organic matter in late Katian and Hirnantian strata in the Valga drill core from southern Estonia (approximately 120 km east of the Viki core) indicate a maximum burial temperature of ~70 °C (Sorci et al., 2020). Acritarch-based thermal alteration index (TAI) and illitization-degree estimates from lower Cambrian strata in northern Estonia suggest even lower values, not higher than ~50 °C (Talyzina, 1998; Talyzina and Moczydłowska, 2000; Kirsimäe et al., 2020), which is in accord with the exceptionally preserved biomarker records from the Ediacaran succession of Baltica (Pehr et al., 2018). Neither PDI nor TAI analyses have been done on the Viki core but excellent preservation of acritarchs in the core rocks is known (Raevskaya and Hints, 2019). Thus, the estimates from the other Estonian sections are reliably applicable to the Viki core.

Further insight into post-depositional processes is provided by Kirsimäe et al. (2020) who reconstructed the burial history in the northern Baltoscandian basin based on clay mineralogy and illitization of smectite. Their results corroborate earlier interpretations and suggest that the burial depth of Ordovician carbonate rocks remained less than 800 m in the study area, and that maximum burial depth was reached during the Late Devonian and Carboniferous. Potassium-Ar dates of mixed-layer illite-smectite and authigenic K-feldspar from Ordovician bentonites fall largely within a period from 420 to 370 Ma in the region including the Viki core (Somelar et al., 2009; Środoń et al., 2009). These include 382 ± 12 and 381 ± 10 Ma K-Ar dates of illite-smectite from the Kinnekulle K-bentonite in the Viki core (Środoń et al., 2009), recording shallow diagenesis largely predating the timing of maximum burial. This illitization is attributed to west-directed fluid migration from the rising Scandinavian Caledonides during the Silurian–Early Devonian Scandian phase of the Caledonian Orogeny (Środoń et al., 2009; Somelar et al., 2009).

Table 1
Instrument parameters for the LA-ICP-MS trace-element mapping and U–Pb dating.

	Trace-element mapping	U–Pb dating
	Analyte Excite 193 nm excimer laser	
Fluence	3 J/cm^2	7 J/cm^2
Beam size	20 μm square; 35 μm square	85 μm circle
Repetition rate	10 Hz	10 Hz
Scan speed	12 μm/s; 20 μm/s	–
He into cell	0.5 L/min	0.28–0.33 L/min
He into cup	0.3 L/min	0.19 L/min
	Agilent 8900 QqQ-ICP-MS	Nu Plasma 3 MC-ICP-MS
RF power	1150 W	1300 W
Coolant gas	15.0 L/min	13.5 L/min
Auxiliary gas	0.9 L/min	0.9 L/min
Ar mixed with carrier gas	0.72 L/min	1.05–1.06 L/min

3. Methods

Two parallel sets of polished thin sections were made of the two samples. The 30-μm-thick thin sections were used for optical petrography and 100-μm-thick sections for backscatter electron (BSE) mapping by SEM, trace-element mapping by LA-quadrupole-ICP-MS, and U–Pb analysis by LA-multicollector-ICP-MS carried out in-sequence. Ten areas in each Viki19-7A and − 27 were first mapped using BSE-SEM and three areas in each were selected for LA-ICP-MS analyses.

3.1. Trace-element mapping by LA-quadrupole-ICP-MS

Trace-element mapping was carried out using a Teledyne-Cetac Analyte Excite 193 nm excimer laser connected to an Agilent 8900 QqQ-ICP-MS. A square laser beam was rastered over three rectangular areas (~1.7–3.8 mm^2) in each thin section, always ablating lines in a left-to-right direction, and with 1 μm overlap between lines to avoid unablated gaps. All areas were initially mapped with a 35 μm-square beam. A smaller part of one of the areas was subsequently mapped with a 20 μm-square beam. Ablations were carried out in a two-volume laser cell within a He atmosphere, and ablated material was transported in a He carrier gas and mixed with Ar just before entering the ICP torch. The following analytes were measured sequentially with 6 ms dwell times on a secondary electron multiplier: ^{24}Mg, ^{28}Si, ^{31}P, ^{43}Ca, ^{55}Mn, ^{56}Fe, ^{88}Sr, ^{139}La, ^{140}Ce, ^{163}Dy, ^{172}Yb, ^{206}Pb, ^{208}Pb, ^{232}Th, and ^{238}U. A smaller subset of these analytes was measured for some of the maps. Other laser and ICP-MS instrument parameters are given in Table 1.

The NIST 612 reference glass was measured between every 7 sample lines and the BHVO-2G reference glass was measured 2–3 times in each sequence. Both glasses were analyzed by rastering over lines (~45–60-s-long for NIST 612 and ~ 40-s-long for BHVO-2G) with the same parameters used on the samples. Pauses of 5–8 s allowed signal washout between lines to avoid carryover of signal between measurements of samples and reference materials.

Data were reduced using a customized version of the "Trace Elements" data reduction scheme in Iolite v. 3.71 (Paton et al., 2011). On-peak baselines were subtracted from the signal on each mass. Calcium-43 was used as an internal elemental standard (assuming 40 wt% Ca for the calcite) to account for differences in ablation yield, aerosol transport, etc. between the different sample and reference material matrices. The NIST 612 reference glass was used to calibrate sensitivity factors for each analyte relative to the internal elemental standard. Trace-element maps were produced using the "Create Image from Selections" tool in Iolite.

The use of an appropriate calibration reference material and internal elemental standard should, in-theory, permit the accurate quantification of elemental concentrations. There are several challenges to quantification that are relevant to the trace element mapping of carbonate: 1)

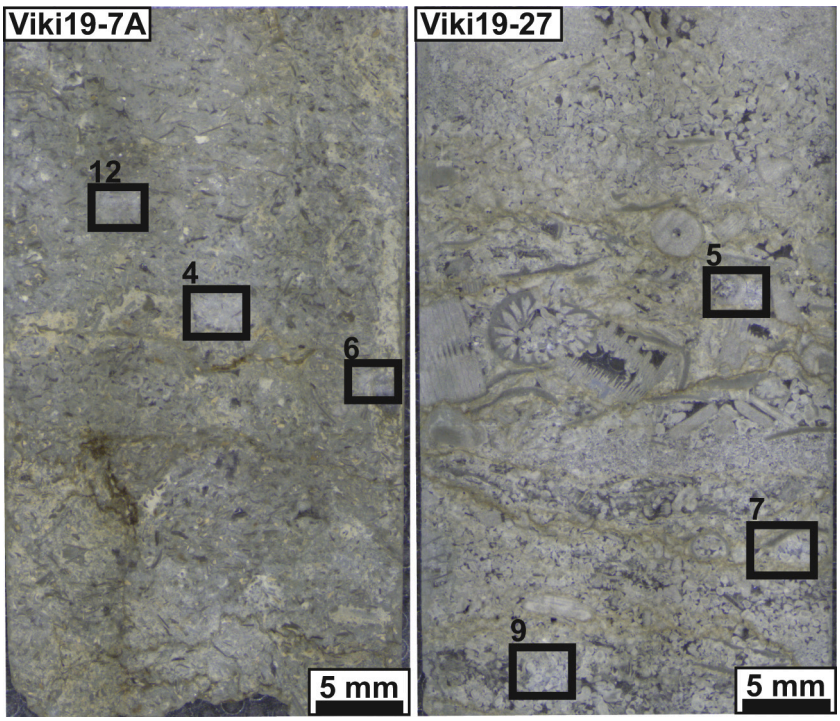

Fig. 3. Scans of thin sections showing areas mapped in detail by SEM-BSE and LA-ICP-MS trace-element mapping (see Fig. 5).

the NIST 612 and BHVO-2G reference glasses, used for calibration and quality control, respectively, are not matrix-matched to carbonate samples; and 2) accurate quantification relies on a known concentration of an internal elemental standard. For an area composed of pure calcite or aragonite, a Ca concentration can be assumed based on stoichiometry of $CaCO_3$. However, if the carbonate phases are solid solutions with dolomite or other components, and 40 wt% Ca is assumed, this will lead to biases in the quantified elemental concentrations. For these reasons, we treat the trace-element maps only qualitatively.

3.2. U–Pb dating by LA-multicollector-ICP-MS

The U–Pb isotopic analyses were done over two analytical sessions using the same LA system connected to a Nu Plasma 3 multicollector-ICP-MS. Thirty-second ablations were preceded by 25–30 s baselines and followed by 5 s washouts. Mercury-202 and ^{204}(Pb + Hg) were measured on secondary electron multipliers, ^{206}Pb and ^{207}Pb were measured on Daly detectors, and ^{232}Th and ^{238}U were measured on Faraday cups with 10^{11}-Ω resistors. Lead-208 was incident on a secondary electron multiplier but was deflected away to prevent tripping the ion counters when encountering large common-Pb signals. Other laser and ICP-MS instrument parameters are given in Table 1.

Measurements of NIST 614 glass, WC-1 reference calcite (Roberts et al., 2017), and two in-house calcite reference materials were measured at the beginning and end of each sequence, as well as between every 5–6 sample measurements. The ASH-15 reference calcite (Nuriel et al., 2020) was also measured in one sequence.

Data were reduced using the "VizualAge UComPbine" data reduction scheme (Chew et al., 2014) in Iolite 4. On-peak baselines were fitted with an "automatic spline" and subtracted from the signal on each channel. The first 2.5 s and last 1 s of signal were trimmed from each measurement. Measurements of NIST 614 were fitted with automatic splines and used to correct for drift in the ^{238}U/^{206}Pb ratio, as well as to normalize ^{207}Pb/^{206}Pb ratios. Due to assumed differences in elemental fractionation behavior between carbonate matrices and glass, no downhole U–Pb fractionation correction was performed, necessitating use of data from the same interval for each measurement (i.e., 2.5 s and 1 s trimmed from the beginning and end, respectively). Further normalization and uncertainty propagation were performed offline. Due to differences in elemental fractionation behavior between glass and carbonate matrices, drift-corrected ^{238}U/^{206}Pb ratios for the calcite measurements required normalization to a reference calcite. The ^{238}U/^{206}Pb of individual analyses were normalized using the common-Pb-anchored (^{207}Pb/^{206}Pb = 0.85) discord lower-intercept date for the WC-1 reference calcite in each sequence relative to a reference age of 254.4 Ma (Roberts et al., 2017). The potential for bias in the U–Pb dates due to inadequate reference material-sample matrix matching (e.g., Guillong et al., 2020) is discussed in Appendix A. An additional 2.5% and 1% were quadratically added to the ^{238}U/^{206}Pb and ^{207}Pb/^{206}Pb ratios, respectively, for each measurement, resulting in MSWD ≅ 1 for regressions in 2-D Terra-Wasserberg space for the two in-house calcite reference materials (see below). Error correlation coefficients (rho) were calculated with internal uncertainties on raw signals using eq. 78 of Schmitz and Schoene (2007).

Concordia diagrams and ages were generated with IsoplotR (Vermeesch, 2018). The ages reported here are unanchored discordia lower-intercept dates, and the uncertainties are 95% confidence intervals scaled by the square root of the MSWD (if MSWD >1) for over-dispersed data. Results for the secondary calcite reference materials are as follows: *ASH-15* (2.965 ± 0.011 Ma; Nuriel et al., 2020) was 2.980 ± 0.350 Ma, $n = 5$, MSWD = 2.7, ^{207}Pb/^{206}Pb$_c$ = 0.840 ± 0.063; *UCSB-436* (11.1 Ma; Kylander-Clark, pers. comm.) was 10.911 ± 0.101 Ma, $n = 44$, MSWD = 0.78, ^{207}Pb/^{206}Pb$_c$ = 0.839 ± 0.002; and *White Pine* (13.0 Ma; Kylander-Clark, Pers. Comm.) was 12.680 ± 0.188 Ma, n = 44, MSWD = 1.6, ^{207}Pb/^{206}Pb$_c$ = 0.697 ± 0.004. The ages reproduced for the secondary reference materials are accurate to within 2.5%. The large uncertainty for ASH-15 is likely due to some combination of the large uncertainties on individual measurements (from very low Pb signals due to the young age) and the fact that only 5 measurements define the discord. The lower-intercept ages for UCSB-436 and White Pine are considerably more precise (≤ 1.5%). To account for systematic uncertainties, for example bias in the age results for the secondary reference calcites and uncertainties in the ages of the reference calcites, an additional blanket uncertainty of 3% was quadratically added to statistical uncertainties of

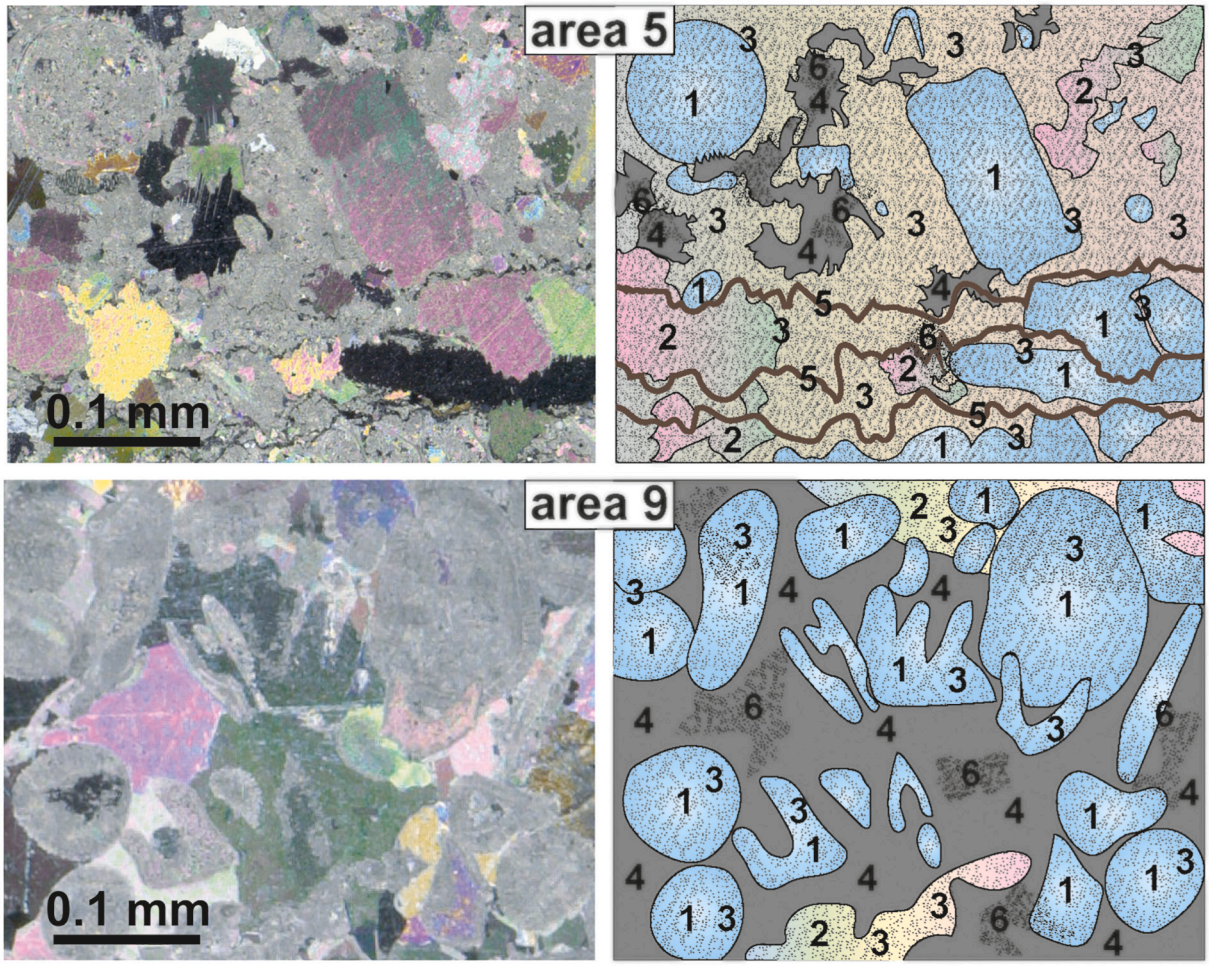

Fig. 4. Optical microscope images in cross polarized light (left panels) and interpretations (right panels) of areas 5 and 9 in sample VIKI19–27 (see Fig. 3 for locations in thin section). Numbering scheme identifies the relative age of petrographic features from oldest (1) to youngest (6): 1 – bioclasts (light blue); 2–3 early stages of cementation (pastel green and pink colors); 4 – late-stage spar cement (grey); 5 – formation of styolites (brown lines); 6 – late micritisation overprinting all features (fine stipple pattern). Note that the 30-μm thin sections come from the complementary billets of the 100-μm thick sections shown in Fig. 3, and so the photomicrographs shown here are not of the exact same areas shown in Fig. 3. (For interpretation of the references to color in this figure legend, the reader is referred to the web version of this article.)

the dates reported for the samples.

4. Results

4.1. Petrography and trace-element characteristics of difference carbonate generations

Samples Viki19-7A and – 27 are bioclastic limestones exhibiting grainstone and packstone textures. Echinoderm fragments are the dominant bioclasts, and ooids and peloids are common (Fig. 3, Fig. 4). Calcitic spar/microspar fills the likely original open-pack grain framework and both grains and cement have undergone variable later micritisation. A younger, clear calcite spar overprints all features, in many places replacing framework grains and leaving only ghost images of original grain constituents. Stylolites cut across all fabrics. In BSE images, calcitic bioclasts are relatively dark due to variable densities of micropores resulting in lower backscatter response, whereas interstitial sparry calcite cements are relatively bright owing to their lower porosity, and in places internal zonation is visible (Fig. 5).

In Viki19–27, grains and cements have distinct trace-element distributions with the latter typically lower in apparent concentrations of Si, Fe, Sr, REE and Th, higher in apparent concentrations of Mn and U, and higher in ratios of Mn/Sr and $^{238}U/^{206}Pb$, although some parts of the spar calcite cement of area 5 (Appendix B in the Supplementary Materials) show higher apparent concentrations of Fe, REE and Th. In Viki19-7A, trace element distributions across the different carbonate generations are less clearly defined. In some areas of each sample, zonation that is only vaguely apparent in BSE images is visible in the trace-element maps. For example, zonation which is vague or invisible in the BSE image is visible in trace element maps of the calcite cement in area 9 of Viki19–27 (Fig. 5a-f). In area 6 of Viki19-7A, some concentric zoning in large replacive spar calcite grains is visible in the BSE image, yet the trace-element (e.g., Ce) zoning is more irregular (Fig. 5h).

4.2. U–Pb dating

The trace-element maps guided placement of U–Pb spot analyses on different textural and compositional generations. The samples are relatively pure limestones with minimal detrital components, which could potentially affect the U–Pb systematics. Still, an effort was made to avoid areas which could contain higher concentrations of detrital components, e.g., stylolites.

Bioclastic grains, regardless of clast type, yield a restricted range in

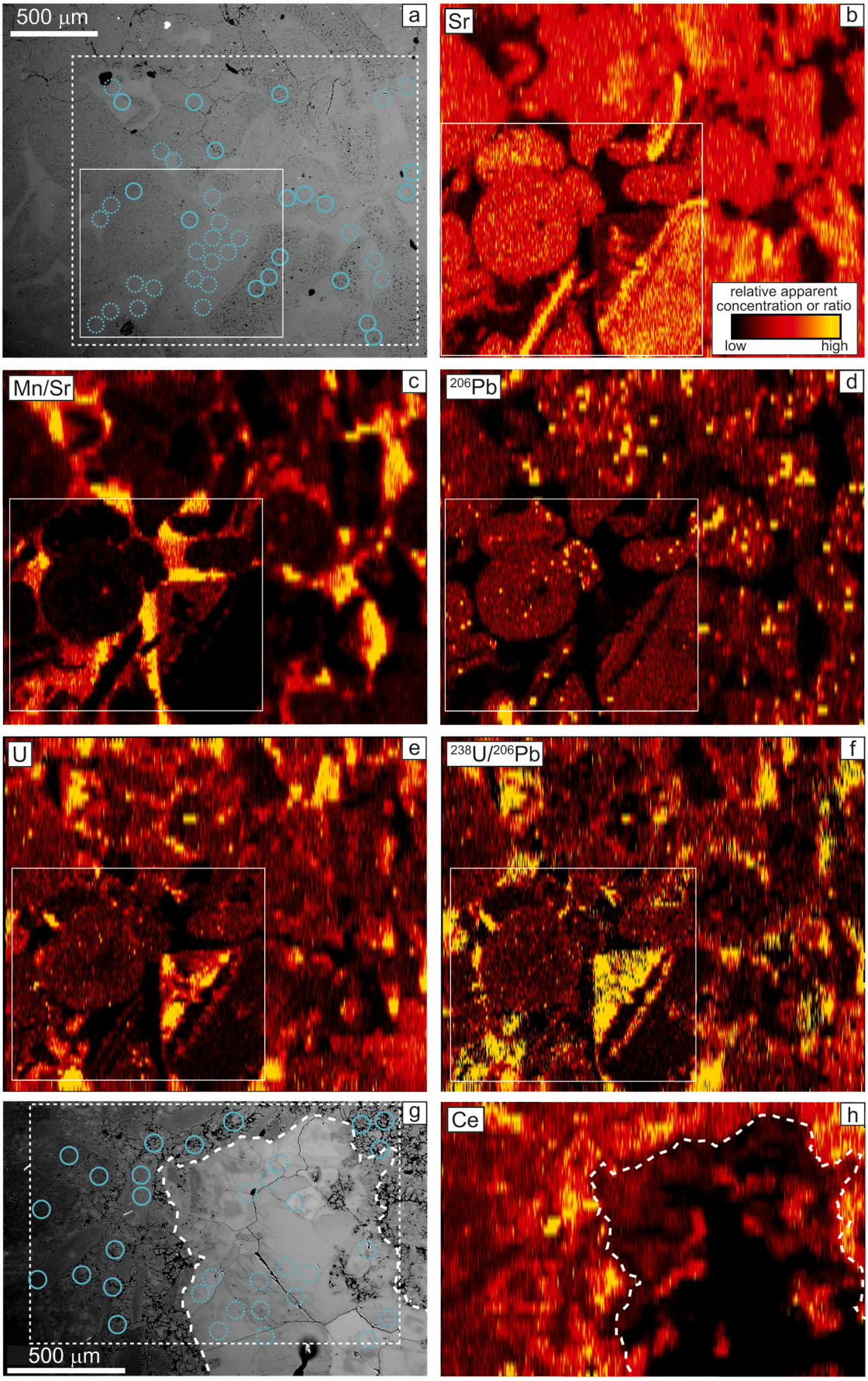

(caption on next page)

Fig. 5. SEM-BSE and trace-element maps for area 9 in Viki19–27 (a-f) and area 6 in Viki19-7A (g-h) (see Fig. 3 for locations). The dashed rectangles on the BSE images show the areas mapped by LA-ICP-MS with a 35 μm beam. The solid rectangle in *a-f* shows a smaller area subsequently mapped at slightly higher resolution with a 20 μm beam. The dashed outline in *g-h* indicates the approximate boundary of BSE-bright, polycrystalline spar calcite. The maps of single elements are relative to ^{43}Ca as an internal elemental standard to account for differences in ablation yield. Maps are considered only qualitatively, but color scales of apparent concentrations and ratios are linear and 'warmer' colors represent higher values. Circles show the locations of subsequent U–Pb spot analyses of different carbonate generations identified as bioclastic grains (solid circles) and interstitial cements (dashed circles). SEM-BSE images showing locations of numbered U–Pb spot analyses and trace-element maps of all areas are provided in Appendix B in the Supplementary Materials.

U/Pb$_c$,[1] with ^{238}U/^{206}Pb < ~6.5 (Fig. 6). Those in Viki19–27 form a broadly colinear array whereas those in Viki19-7A display more scatter. Due to the limited spread in U/Pb$_c$, analyses of bioclastic grains in each sample do not yield precise lower-intercept dates. Excluding seven analyses that form a roughly horizontal (variable ^{238}U/^{206}Pb) array on a concordia diagram (Fig. 6), bioclastic grains in Viki19-7A yield a lower-intercept date of 459 ± 45/47 Ma (statistical uncertainty on regression/including propagated 3% uncertainty, MSWD = 13.0, ^{207}Pb/^{206}Pb$_c$ = 0.800, n = 50/57 total analyses). Bioclastic grains in Viki19–27 yield a lower-intercept date of 428 ± 15/19 Ma (MSWD = 2.4, ^{207}Pb/^{206}Pb$_c$ = 0.839, n = 46/46).

Analyses of interstitial cements have a wider range in U/Pb$_c$, with ^{238}U/^{206}Pb up to ~15.7, thereby yielding more precise lower-intercept dates. Including all analyses, these generations in Viki19-7A yield a lower-intercept date of 412 ± 7/14 Ma (MSWD = 8.4, ^{207}Pb/^{206}Pb$_c$ = 0.765, n = 54/54), and those in Viki19–27 yield a lower-intercept date of 414 ± 5/14 Ma (MSWD = 4.1, ^{207}Pb/^{206}Pb$_c$ = 0.827, n = 62/62). Individual common-Pb-corrected ^{206}Pb/^{238}U dates from analyses with ^{238}U/^{206}Pb > 6.5 from both samples range from ca. 376–485 Ma, with a weighted mean of ca. 414 Ma and MSWD = 11.8 for 56 analyses (Fig. 7).

5. Discussion

5.1. Trace element characteristics of the different carbonate generations

Bioclastic grains and cements in the samples are distinguishable optically and in BSE images, and additional details are revealed in trace-element maps. Interstitial calcite cement displays various characteristics of diagenetic calcite, in-particular low Sr and elevated Mn/Sr (Fig. 5b-c), whereas bioclastic grains retain more primary marine-carbonate trace-element characteristics (e.g., high Sr).

It has been recognized in at least some cases that U/Pb ratios are decreased during carbonate diagenesis due to expulsion of U during recrystallization (e.g., Jones et al., 1995), and it has been suggested that this is a common feature of carbonates modified by diagenesis (Kaurova et al., 2010). Rasbury and Cole (2009) and Roberts et al. (2020) reveal much more variability in the U/Pb$_c$ of various types of carbonate, and the latter conclude that predicting the U/Pb$_c$ of a particular type of carbonate prior to analysis is challenging or impossible. The bioclastic grains in the samples from our study display a rather restricted range of U/Pb$_c$. The spar calcite cement has variable U/Pb$_c$, overlapping with the low U/Pb$_c$ of grains but also extending to relatively high U/Pb$_c$ (Fig. 5f, Fig. 6). In some areas, high U/Pb$_c$ corresponds to relatively low U concentrations indicating that variability in common-Pb content also partially controls the observed U/Pb$_c$ (Fig. 5e-f). Regardless of the combination of U-partitioning and Pb-expulsion leading to the high U/Pb$_c$ of interstitial calcite cement, these processes did not pervasively affect the bioclastic grains.

5.2. Interpretation of the lower-intercept dates and over-dispersion

The analyses included in each of the lower-intercept and weighted mean common-Pb-corrected dates are over-dispersed and yield MSWD >1 following uncertainty propagation. Possible explanations for this include: 1) independent mobilization of U and/or Pb within or among phases long after crystallization of the different carbonate generations (e.g., recent Pb- or U-loss); 2) ancient *partial* resetting of the U–Pb systematics through recrystallization and/or intracrystalline diffusion of U and/or Pb in the carbonate bioclasts and pre-existing carbonate cement in the pore spaces; and 3) mixed sampling of bioclastic grains and cement generations of different age during ablation. The first scenario cannot be entirely ruled out. Several analyses of bioclastic grains in sample Viki19-7A (those excluded from the regression in Fig. 6) deviate to higher ^{238}U/^{206}Pb values from a more nearly colinear array with a lower-intercept date consistent with the deposition age. Such a trajectory could potentially be explained by recent Pb-loss or U-gain. However, there are few other analyses in the samples that so obviously deviate from the near-colinear arrays which yield lower-intercept dates consistent with the depositional ages of the samples and an apparent slightly younger (ca. 414–412 Ma) age component. Several analyses of calcite cement in Viki19-7A fall to the left of the ca. 412 Ma isochron, but most are enveloped by the deposition-age reference isochron and can be explained by mixing between the depositional age and younger (perhaps ca. 412 Ma) age components.

Differentiating between the other scenarios is not possible with existing data but, in either case, the discordia lower-intercept dates (ca. 414–412 Ma) and the weighted-mean common-Pb-corrected date (ca. 414 Ma) calculated for the cements would represent mixed ages between older (presumably depositional) and younger (cementation) age components. Thus, they likely constrain a *maximum* rather than *absolute* timing of cementation. The youngest common-Pb-corrected dates imply (re)crystallization as late as ca. 376 Ma (Fig. 7). The few common-Pb-corrected dates older than the depositional ages of the samples have relatively low U/Pb$_c$ and are therefore leveraged more by the common-Pb composition used for the correction. The younger common-Pb-corrected dates are nearer to concordia and, thus, are leveraged less by the common-Pb composition used for the correction.

The U–Pb systematics of bioclastic grains may also have been reset during diagenesis. In this case, the low U/Pb$_c$ in the clasts compared to the calcite cement may be due to differences in elemental partitioning between the clast and cement phases. Indeed, the common-Pb compositions of the different generations in each sample are similar, despite differences between the two samples. Nevertheless, the relatively low U/Pb$_c$ and limited spread among individual analyses results in imprecise lower-intercept dates for bioclastic grains which are not strictly resolvable from either the deposition ages or lower-intercept dates of the late-stage calcite cement. The calcite cement is, however, resolvably younger than the biostratigraphically constrained depositional ages of the samples (Fig. 6, Fig. 7).

5.3. The timing of diagenetic calcite (re)crystallization and its implications

Despite the inability to assign a discrete absolute age to the timing of diagenesis—as discussed above—we interpret ca. 414–376 Ma as the probable time interval during which the interstitial calcite cement formed or recrystallized, which postdates the biostratigraphically constrained depositional age by at least several tens of millions of years (Fig. 6, Fig. 7). Petrographic analyses and trace-element heterogeneities imply multiple phases and zonation of cements but whether those

[1] Note that U/Pb$_c$ (the ratio of uranium to common-Pb) is commonly expressed as "μ" = ^{238}U/^{204}Pb. Because we do not report ^{204}Hg-corrected ^{204}Pb data, we refer simply to U/Pb$_c$, which corresponds the position of the analysis along the regressions in Terra-Wasserburg space or "near-concordance".

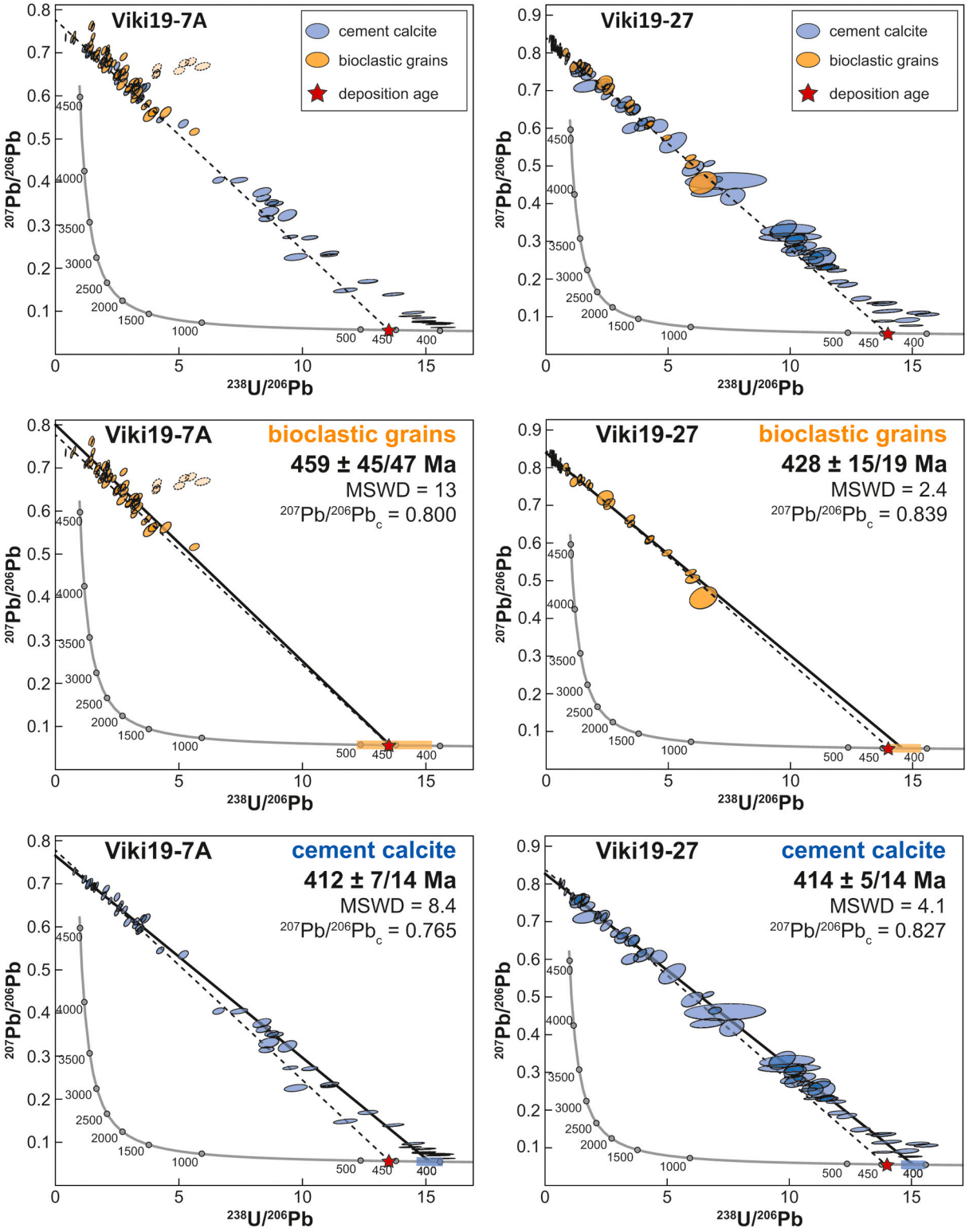

Fig. 6. Terra-Wasserburg concordia diagrams for each sample with categorization of different carbonate generations and corresponding intercept dates. Dashed lines are visually defined reference isochrons for the depositional ages of the samples and hypothetical common-Pb compositions and are not meant to represent precise regressions. Solid lines are unanchored "model-1" regressions calculated with IsoplotR (Vermeesch, 2018). The two uncertainties given for each lower-intercept date are the statistical uncertainties on the regressions (first number) and the full uncertainties including the quadratically added 3% blanket uncertainties. Color bands along concordia at the lower intercepts show the full uncertainties on the dates including the blanket 3% uncertainty. Semi-transparent ellipses with dashed outlines were excluded from the regression of analyses of bioclastic grains in Viki19-7A.

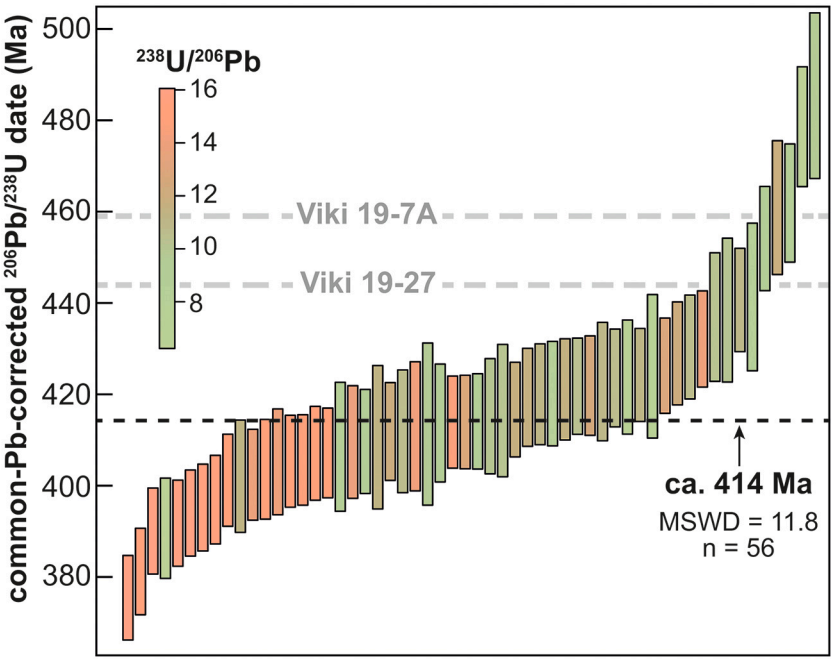

Fig. 7. Common-Pb-corrected $^{206}Pb/^{238}U$ dates for individual analyses with $^{238}U/^{206}Pb > 6.5$ from both samples. Analyses are corrected using the common-Pb composition from unanchored regressions of all interstitial cement data. The threshold $^{238}U/^{206}Pb > 6.5$ is used as an arbitrary cutoff to highlight analyses with the most radiogenic compositions, which are leveraged less by the common-Pb composition used for the correction. Five analyses with uncertainties >5% on common-Pb-corrected dates are excluded. Dashed black line is the weighted-mean of the dates; note that the MSWD > > 1 indicates that the dates do not define a single population, and thus the weighted-mean date should not be interpreted as an absolute age. For this reason, the *date* is given as ca. 414 Ma with no uncertainty interval. Dashed grey lines show the depositional age of each sample.

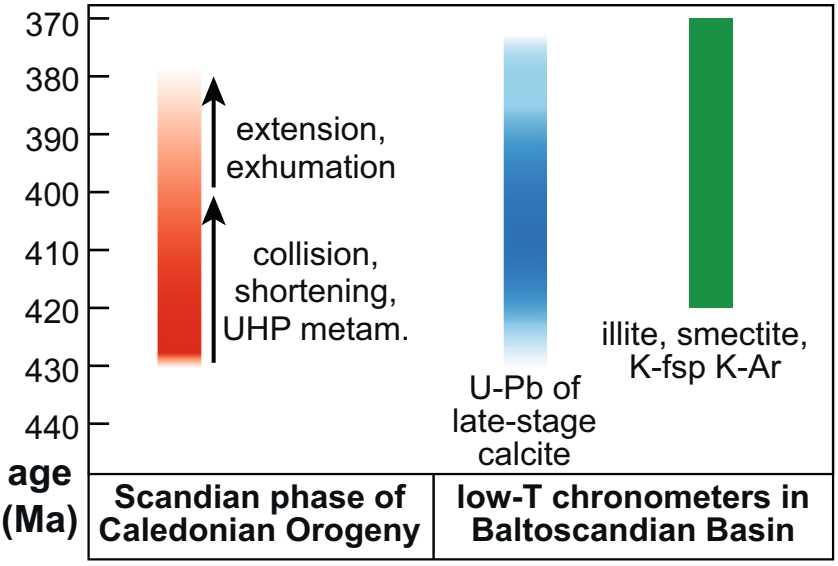

Fig. 8. Timeline showing the range of calcite U–Pb, and illite-smectite and K-feldspar K–Ar dates (from Somelar et al., 2009; Środoń et al., 2009) relative to the timing of Scandian phase of the Caledonian orogeny (from Corfu et al., 2014). The shading gradient of the band for the Scandian record represents the progression from collision to orogenic collapse of the Caledonian orogen. The shading gradient of the band for the calcite U–Pb record represents—qualitatively—uncertainty of the absolute timing or duration of post-depositional calcite (re)crystallization as discussed in the text.

formed over a protracted time interval or as a discrete event is not resolvable. This episode—or period— may have also affected the bioclastic carbonate grains, although not sufficiently to thoroughly redistribute major and trace elements across the different carbonate phases nor to fully modify the U/Pb of the grains.

The probable age range (ca. 414–376 Ma) of the diagenetic calcite largely overlaps the 420–370 Ma K-Ar dates for illite-smectite and authigenic K-feldspar formation found throughout the Baltoscandian basin (Somelar et al., 2009; Środoń et al., 2009), attributed to the Scandian phase (ca. 430–380 Ma; Corfu et al., 2014) of the Caledonian orogeny (Fig. 8). Hence, the most likely genesis of diagenetic (re)crystallization of interstitial calcite cement was in response to fluid flow driven through the basin by Caledonian orogenesis, as suggested by Somelar et al. (2009) and Środoń et al. (2009). The Viki borehole is more than 600 km inboard (in the direction of vergence) of the present-day extent of the Caledonian nappes of Norway and Sweden, and it is possible that the timing overlap between orogenesis and (re) crystallization is coincidental. However, Środoń et al. (2009) and Somelar et al. (2010) noted that illitization occurred across a broad zone that includes the Viki borehole and that this occurred at shallow depths, prior to the timing of maximum burial. Our data are in agreement with that scenario.

These findings highlight a key implication for geochemical proxy data, namely, how to assess whether the processes and environmental conditions revealed by those data were established at the time of deposition or at the time of diagenesis, or reflect a mixture of both. Stable isotope and elemental ratio data on carbonate rocks are often obtained on bulk-rock samples, typically to deduce original (i.e., depositional) redox conditions and isotope values. This work using spatially resolved U–Pb spot analyses offers a case-in-point and underscores the necessity for careful petrographic, imaging, and trace-element mapping to inform what components of a carbonate rock are being analyzed for environmental proxies and to confirm age similarities or differences. For the well-preserved Ordovician carbonate rocks sampled in the Viki core,

the timing of sedimentation versus that of diagenetic carbonate recrystallization was tens of millions of years apart, hence geochemical data derived from bulk-rock analyses may represent mixing of vastly different geochemical and environmental ancestries. Interestingly, the global Hirnantian carbon isotope excursion, as well as other widely developed Ordovician and Silurian isotopic events, are clearly recorded in the Viki borehole (Hints et al., 2014; Kaljo et al., 2003). Thus, it seems that late diagenesis has not thoroughly obscured the C isotope record. In contrast, S isotope trends reported from the early Silurian strata of the Viki core (Richardson et al., 2019) suggest mixed patterns likely due to early diagenetic overprints. Our findings indicate that late diagenetic effects should also be considered. Lastly, due to calcite's reactivity and propensity for recrystallization, we emphasize the potential of the calcite U–Pb system as a chronometer of low-temperature diagenetic processes to be used in conjunction with other low-temperature chronometers such as K–Ar in diagenetic silicate minerals.

6. Conclusions

We applied LA-ICP-MS trace-element mapping and U–Pb geochronology on primary bioclastic grains and interstitial carbonate cementation phases in two samples of well-preserved Ordovician rocks recovered from the Viki core on Saaremaa island, Estonia. The grains and cements can be readily differentiated optically and in BSE images, as well as via distinct trace-element characteristics from LA-ICP-MS mapping. Bioclastic carbonate grains have a restricted range in U/Pb_c and thus yield imprecise discordia lower-intercept dates but, nonetheless, are within uncertainty of the timing of deposition as established from biostratigraphic correlations. The diagenetic interstitial calcite cements have higher U/Pb_c and yield more precise lower-intercept dates of ca. 414–412 Ma. These likely represent mixed ages, and individual common-Pb-corrected dates extend to ca. 376 Ma. Consequently, the absolute timing of diagenetic calcite (re)crystallization remains imprecise but likely occurred between ca. 414 and 376 Ma, an age range that overlaps with the timing of illitization as deduced from K–Ar dates from K-bentonites across the Baltoscandian basin. The most likely driver of these temporally coincident diagenetic phases was far-field fluid migration in response to orogenesis during formation of the Scandinavian Caledonides.

Our results bring into sharp focus the necessity of identifying which components of a carbonate rock (e.g., framework grains versus cements) are being analyzed when obtaining geochemical and isotopic proxy data aimed at deducing environmental conditions at the time of deposition. As the Viki core samples we analyzed show that the timing of diagenetic calcite (re)crystallization occurred several tens of millions of years following sedimentation, circumspection is needed when interpreting the significance of isotopic and elemental ratio trends and patterns when such data are derived purely from bulk analyses of carbonate rocks.

Declaration of Competing Interest

The authors declare that they have no known competing financial interests or personal relationships that could have appeared to influence the work reported in this paper.

Acknowledgements

The LA-ICP-MS analyses for this study were performed in the Norwegian Laboratory for Mineral and Materials Characterisation (MiMaC) NGU node, supported by the Research Council of Norway project number 269842/F50. OH and AL are grateful for the support from the Estonian Research Council Grant PRG836. The manuscript was improved based on feedback from two anonymous reviewers, and Dhilip Kumar and Claudia Romano are thanked for editorial handling.

Supplementary data

Supplementary data to this article can be found online at https://doi.org/10.1016/j.chemgeo.2021.120563.

References

Ainsaar, L., Kaljo, D., Martma, T., Meidla, T., Männik, P., Nõlvak, J., Tinn, O., 2010. Middle and Upper Ordovician carbon isotope chemostratigraphy in Baltoscandia: a correlation standard and clues to environmental history. Palaeogeogr. Palaeoclimatol. Palaeoecol. 294, 189–201. https://doi.org/10.1016/j.palaeo.2010.01.003.

Ballo, E.G., Augland, L.E., Hammer, Ø., Svensen, H.H., 2019. A new age model for the Ordovician (Sandbian) K-bentonites in Oslo, Norway. Palaeogeogr. Palaeoclimatol. Palaeoecol. 520, 203–213. https://doi.org/10.1016/j.palaeo.2019.01.016.

Bathurst, R.G.C., 1976. Carbonate Sediments and their Diagenesis, Second ed. Elsevier Publishing, Amsterdam, The Netherlands.

Bergström, S. M., Toprak, F. Ö., Huff, W. D., Mundil, R., 2008. Implications of a new, biostratigraphically well-controlled, radio-isotopic age for the lower Telychian Stage of the Llandovery Series (Lower Silurian, Sweden). Episodes 31, 309–314. Doi:10.18814/epiiugs/2008/v31i3/004.

Brand, U., Veizer, J., 1980. Chemical diagenesis of a multicomponent carbonate system – 1. Trace elements. J. Sediment. Petrol. 50, 1219–1236. https://doi.org/10.1306/212F7BB7-2B24-11D7-8648000102C1865D.

Chew, D.M., Petrus, J.A., Kamber, B.S., 2014. U–Pb LA–ICPMS dating using accessory mineral standards with variable common Pb. Chem. Geol. 363, 185–199.

Cocks, L.R.M., Torsvik, T.H., 2005. Baltica from the late Precambrian to mid-Palaeozoic times: the gain and loss of a terrane's identity. Earth Sci. Rev. 72, 39–66. https://doi.org/10.1016/j.earscirev.2005.04.001.

Cocks, L.R.M., Torsvik, T.H., 2020. Ordovician palaeogeography and climate change. Gondwana Res. https://doi.org/10.1016/j.gr.2020.09.008.

Corfu, F., Andersen, T.B., Gasser, D., 2014. The Scandinavian Caledonides: main features, conceptual advances and critical questions. Geol. Soc. Lond., Spec. Publ. 390 (1), 9–43.

Derry, L.A., 2010. A burial diagenesis origin for the Ediacaran Shuram–Wonoka carbon isotope anomaly. Earth Planet. Sci. Lett. 294 (1), 152–162.

Drost, K., Chew, D., Petrus, J.A., Scholze, F., Woodhead, J.D., Schneider, J.W., Harper, D. A., 2018. An image mapping approach to U–Pb LA-ICP-MS carbonate dating and applications to direct dating of carbonate sedimentation. Geochem. Geophys. Geosyst. 19 (12), 4631–4648.

Godeau, N., Deschamps, P., Guihou, A., Leonide, P., Tendil, A., Gerdes, A., Girard, J.P., 2018. U–Pb dating of calcite cement and diagenetic history in microporous carbonate reservoirs: Case of the Urgonian Limestone, France. Geology 46 (3), 247–250.

Goldman, D., Sadler, P.M., Leslie, S.A., 2020. Chapter 20. The Ordovician Period. In: Gradstein, F.M., Ogg, J.G., Schmitz, M.D., Ogg, G.M. (Eds.), Geologic Time Scale 2020. Volume 2 (pp. 631–694). Elsevier. https://doi.org/10.1016/B978-0-12-824360-2.00020-6.

Guillong, M., Wotzlaw, J.F., Looser, N., Laurent, O., 2020. Evaluating the reliability of U–Pb laser ablation inductively coupled plasma mass spectrometry (LA-ICP-MS) carbonate geochronology: matrix issues and a potential calcite validation reference material. Geochronology 2 (1), 155–167.

Hints, O., Martma, T., Männik, P., Nõlvak, J., Põldvere, A., Shen, Y., Viira, V., 2014. New data on Ordovician stable isotope record and conodont biostratigraphy from the Viki reference drill core, Saaremaa Island, western Estonia. GFF 136, 100–104. https://doi.org/10.1080/11035897.2013.873989.

Jaanusson, V., 1976. Faunal dynamics in the Middle Ordovician (Viruan) of Balto-Scandia. In: Bassett, M.G. (Ed.), The Ordovician System: Proceedings of a Palaeontological Association Symposium. University of Wales Press, Cardiff, pp. 301–326.

Jaanusson, V., 1995. Confacies differentiation and upper Middle Ordovician correlation in the Baltoscandian basin. Proceedings of the Estonian Academy of Sciences. Geology 44, 73–86.

Jeppsson, L., Männik, P., 1993. High-resolution correlations between Gotland and Estonia near the base of the Wenlock. Terra Nova 5, 348–358. https://doi.org/10.1111/j.1365-3121.1993.tb00268.x.

Jones, C.E., Halliday, A.N., Lohmann, K.C., 1995. The impact of diagenesis on high-precision UPb dating of ancient carbonates: an example from the late Permian of New Mexico. Earth Planet. Sci. Lett. 134 (3–4), 409–423.

Kaljo, D., Martma, T., Männik, P., Viira, V., 2003. Implications of Gondwana glaciations in the Baltic late Ordovician and Silurian and a carbon isotopic test of environmental cyclicity. Bull. Soc. Geol. Fr. 174, 59–66. https://doi.org/10.2113/174.1.59.

Kaurova, O.K., Ovchinnikova, G.V., Gorokhov, I.M., 2010. U-Th-Pb systematics of Precambrian carbonate rocks: dating of the formation and transformation of carbonate sediments. Stratigr. Geol. Correl. 18 (3), 252–268.

Kiipli, T., Kallaste, T., Nestor, V., Loydell, D.K., 2010. Integrated Telychian (Silurian) K-bentonite chemostratigraphy and biostratigraphy in Estonia and Latvia. Lethaia 43 (1), 32–44.

Kirsimäe, K., Somelar, P., Jõeleht, A., 2020. Illitization of the lower Cambrian (Terreneuvian) Blue Clay in the northern Baltic Palaeobasin. Estonian J. Earth Sci. 69, 200–213. https://doi.org/10.3176/earth.2020.14.

Lehnert, O., Männik, P., Joachimski, M.M., Calner, M., Frýda, J., 2010. Palaeoclimate perturbations before the Sheinwoodian glaciation: A trigger for extinctions during

the 'Ireviken Event.'. Palaeogeogr. Palaeoclimatol. Palaeoecol. 296, 320–331. https://doi.org/10.1016/j.palaeo.2010.01.009.
Männil, R., 1966. Evolution of the Baltic basin during the Ordovician. Valgus, Tallinn 201.
Nehring-Lefeld, M., Modliński, Z., Swadowska, E., 1997. Thermal evolution of the Ordovician in the western margin of the East-European Platform: CAI and Ro data. Geological Quarterly 41, 129–138.
Nestor, V., 2005. Chitinozoans of the Margachitina margaritana Biozone and the Llandovery-Wenlock boundary in West Estonian drill cores. Proceedings of the Estonian Academy of Sciences. Geology 54, 87–111.
Nestor, V., Einasto, R., 1997. Correlation of some Wenlock outcrop sections of Gotland with the Ohesaare section of Saaremaa, Estonia. In Proceedings of the Estonian Academy of Sciences, Geology (Vol. 46, no. 4, pp. 155-168). Estonian Academy Publishers. 46 (4), 155–168.
Nõlvak, J., Hints, O., Männik, P., 2006. Ordovician timescale in Estonia: recent developments. Proceedings of the Estonian Academy of Sciences. Geology 55, 95–108.
Nuriel, P., Wotzlaw, J.F., Ovtcharova, M., Vaks, A., Stremtan, C., Šala, M., Roberts, N.M. W., Kylander-Clark, A.R., 2020. The use of ASH-15 flowstone as a matrix-matched reference material for laser-ablation U–Pb geochronology of calcite. Geochronology Discussions 1–26.
Paton, C., Hellstrom, J., Paul, B., Woodhead, J., Hergt, J., 2011. Iolite: Freeware for the visualisation and processing of mass spectrometric data. J. Anal. At. Spectrom. 26 (12), 2508–2518.
Pehr, K., Love, G.D., Kuznetsov, A., Podkovyrov, V., Junium, C.K., Shumlyanskyy, L., Sokur, T., Bekker, A., 2018. Ediacara biota flourished in oligotrophic and bacterially dominated marine environments across Baltica. Nat. Commun. 9, 1–10. https://doi.org/10.1038/s41467-018-04195-8.
Põldvere, Anne (Ed.), 2010. Viki Drill Core. Estonian Geological Sections Bulletin, vol. 10. Geological Survey of Estonia, Tallinn, 56 pp.
Raevskaya, E.G., Hints, O., 2019. Acritarchs from the Middle and Upper Ordovician of Estonia and their stratigraphic implications, in: 13th International Symposium on the Ordovician System: Contributions of International Symposium. Novosibirsk, Russia (July 19–22, 2019). Publishing House of SB RAS. Novosibirsk 165–168.
Rasbury, E.T., Cole, J.M., 2009. Directly dating geologic events: U–Pb dating of carbonates. Rev. Geophys. 47 (3).
Richardson, J.A., Keating, C., Lepland, A., Hints, O., Bradley, A.S., Fike, D.A., 2019. Silurian records of carbon and sulfur cycling from Estonia: the importance of depositional environment on isotopic trends. Earth Planet. Sci. Lett. 512, 71–82. https://doi.org/10.1016/j.epsl.2019.01.055.
Roberts, N.M., Walker, R.J., 2016. U–Pb geochronology of calcite-mineralized faults: absolute timing of rift-related fault events on the Northeast Atlantic margin. Geology 44 (7), 531–534.
Roberts, N.M., Rasbury, E.T., Parrish, R.R., Smith, C.J., Horstwood, M.S., Condon, D.J., 2017. A calcite reference material for LA-ICP-MS U–Pb geochronology. Geochem. Geophys. Geosyst. 18 (7), 2807–2814.
Roberts, N.M., Drost, K., Horstwood, M.S., Condon, D.J., Chew, D., Drake, H., Lee, J.K., 2020. Laser ablation inductively coupled plasma mass spectrometry (LA-ICP-MS) U–Pb carbonate geochronology: strategies, progress, and limitations. Geochronology 2 (1), 33–61.
Rose, C.V., Fischer, W.W., Finnegan, S., Fike, D.A., 2019. Records of carbon and sulfur cycling during the Silurian Ireviken Event in Gotland. Geochim. Cosmochim. Acta 246, 299–316.
Schmitz, M.D., Schoene, B., 2007. Derivation of isotope ratios, errors, and error correlations for U–Pb geochronology using 205Pb-235U-(233U)-spiked isotope dilution thermal ionization mass spectrometric data. Geochem. Geophys. Geosyst. 8 (8).
Smith, P.E., Farquhar, R.M., Hancock, R.G., 1991. Direct radiometric age determination of carbonate diagenesis using U–Pb in secondary calcite. Earth Planet. Sci. Lett. 105 (4), 474–491.
Somelar, P., Kirsimäe, K., Środoń, J., 2009. Mixed-layer illite-smectite in the Kinnekulle K-bentonite, northern Baltic basin. Clay Miner. 44, 455–468. https://doi.org/10.1180/claymin.2009.044.4.455.
Somelar, P., Kirsimäe, K., Hints, R., Kirs, J., 2010. Illitization of early Paleozoic K-Bentonites in the Baltic basin: decoupling of burial- and fluid-driven processes. Clay Clay Miner. 58, 388–398. https://doi.org/10.1346/CCMN.2010.0580309.
Sorci, A., Cirilli, S., Clayton, G., Corrado, S., Hints, O., Goodhue, R., Schito, A., Spina, A., 2020. Palynomorph optical analyses for thermal maturity assessment of Upper Ordovician (Katian-Hirnantian) rocks from Southern Estonia. Mar. Pet. Geol. 120, 104574. https://doi.org/10.1016/j.marpetgeo.2020.104574.
Środoń, J., Clauer, N., Huff, W., Dudek, T., Banaś, M., 2009. K-Ar dating of the lower Palaeozoic K-bentonites from the Baltic basin and the Baltic Shield: implications for the role of temperature and time in the illitization of smectite. Clay Miner. 44, 361–387. https://doi.org/10.1180/claymin.2009.044.3.361.
Swart, P.K., 2015. The geochemistry of carbonate diagenesis: the past, present and future. Sedimentology 62 (5), 1233–1304.
Talyzina, N.M., 1998. Fluorescence intensity in early Cambrian acritarchs from Estonia. Rev. Palaeobot. Palynol. 100, 99–108. https://doi.org/10.1016/S0034-6667(97)00059-6.
Talyzina, N.M., Moczydłowska, M., 2000. Morphological and ultrastructural studies of some acritarchs from the lower Cambrian Lükati Formation, Estonia. Rev. Palaeobot. Palynol. 112, 1–21. https://doi.org/10.1016/S0034-6667(00)00032-4.
Tonarová, P., Hints, O., Eriksson, M.E., 2014. Impact of the Silurian Ireviken Event on polychaete faunas: new insights from the Viki drill core, western Estonia. GFF 136, 270–274. https://doi.org/10.1080/11035897.2013.862855.
Vermeesch, P., 2018. IsoplotR: a free and open toolbox for geochronology. Geosci. Front. 9 (5), 1479–1493.